Single-particle fluorescence tracking combined with TrackMate assay reveals highly heterogeneous and discontinuous lysosomal transport in freely orientated axons

Yongyang Liu[1], Yaxin Lu[1], Zhiyong Tang[1], Yuheng Cao[2], Dehua Huang[3], Feng Wu[3], Yejun Zhang[3], Chunyan Li[4], Guangcun Chen[4], and Qiangbin Wang[5]

[1]University of Science and Technology of China
[2]ShanghaiTech University
[3]Suzhou Institute of Nano-tech and Nano-Bionics Chinese Academy of Sciences
[4]Suzhou Institute of Nano-tech and Nano-bionics
[5]Affiliation not available

January 14, 2022

Abstract

Axonal transport plays a significant role in the establishment of neuronal polarity, axon growth, and synapse formation during neuronal development. The axon of a naturally growing neuron is a highly complex and multifurcated structure with a large number of bends and branches. Nowadays, the study of dynamic axonal transport in morphologically complex neurons is greatly limited by the technological barrier. Here, a sparse gene transfection strategy was developed to locate fluorescent mCherry in the lysosome of primary neurons, thus enabling us to track the lysosome-based axonal transport with a single-particle resolution. Thereby, several axonal transport models were observed, including forward or backward transport model, stop-and-go model, repeated back-and-forth transport model, and cross-branch transport model. Then, the accurate single-particle velocity quantification by TrackMate revealed a highly heterogeneous and discontinuous transportation process of lysosome-based axonal transport in freely orientated axons. And, multiple physical factors, such as the axonal structure and the size of particles, were disclosed to affect the velocity of particle transporting in freely orientated axons. The combined single-particle fluorescence tracking and TrackMate assay can be served as a facile tool for evaluating axonal transport in neuronal development and axonal transport-related diseases.

Research Article

Single-particle fluorescence tracking combined with TrackMate assay revealshighly heterogeneous and discontinuouslysosomal transport in freely orientated axons

Yongyang Liu[1,2,#], Yaxin Lu[1,2,#], Zhiyong Tang[1,2], Yuheng Cao[2,3], Dehua Huang[1], Feng Wu[1], Yejun Zhang[1], Chunyan Li[1,2], Guangcun Chen[1,2,], Qiangbin Wang[1,2,3,4]*

[1]School of Nano-Tech and Nano-Bionics, University of Science and Technology of China, Hefei 230026, China

[2]CAS Key Laboratory of Nano-Bio Interface, Suzhou Key Laboratory of Functional Molecular Imaging Technology, Division of Nanobiomedicine and *i* -Lab, Suzhou Institute of Nano-Tech and Nano-Bionics, Chinese Academy of Sciences, Suzhou 215123, China

[3]School of Physical Science and Technology, ShanghaiTech University, Shanghai 201210, China

[4]College of Materials Sciences and Opto-Electronic Technology, University of Chinese Academy of Sciences, Beijing 100049, China

[#]These authors contributed equally to this work.

Correspondence: Prof. Guangcun Chen, Division of Nanobiomedicine and i -Lab, Suzhou Institute of Nano-Tech and Nano-Bionics, Chinese Academy of Sciences, Suzhou 215123, China.

E-mail: gcchen2011@sinano.ac.cn

Keywords: fluorescence imaging, axonal transport, lysosomal transport, TrackMate, single-particle tracking

Abstract

Axonal transport plays a significant role in the establishment of neuronal polarity, axon growth, and synapse formation during neuronal development. The axon of a naturally growing neuron is a highly complex and multifurcated structure with a large number of bends and branches. Nowadays, the study of dynamic axonal transport in morphologically complex neurons is greatly limited by the technological barrier. Here, a sparse gene transfection strategy was developed to locate fluorescent mCherry in the lysosome of primary neurons, thus enabling us to track the lysosome-based axonal transport with a single-particle resolution. Thereby, several axonal transport models were observed, including forward or backward transport model, stop-and-go model, repeated back-and-forth transport model, and cross-branch transport model. Then, the accurate single-particle velocity quantification by TrackMate revealed a highly heterogeneous and discontinuous transportation process of lysosome-based axonal transport in freely orientated axons. And, multiple physical factors, such as the axonal structure and the size of particles, were disclosed to affect the velocity of particle transporting in freely orientated axons. The combined single-particle fluorescence tracking and TrackMate assay can be served as a facile tool for evaluating axonal transport in neuronal development and axonal transport-related diseases.

1. Introduction

Axonal transport serves as a cytoplasm trafficker during neuronal development, playing a significant role in the establishment of neuronal polarity, axon growth and stability, and synapse formation.[1] The cytoplasm trafficker represents cargoes varying from every type of membranous organelle and vesicles such as lysosome, mitochondria, endosome, to non-membranous cargoes like cytosolic protein complexes, mRNAs, cytoskeletal polymers, and ribosomes.[2-4]Lysosomes have long been viewed as housekeeping organelles responsible for endocytic and autophagic component degradation, thus maintaining cellular homeostasis in the neuron. The latest research indicates that a small rat sarcoma virus-related GTPase (Rab2) mediates dense core vesicles biogenesis and endosome-lysosome fusion,[5]via Rab2, activated by the upstream regulator endosomal membrane protein, directly or indirectly assisting lysosomal motility factor Arl8,[6]activated by the upstream regulator BORC,[7] to recruit kinesin motor proteins.[8]Moreover, not like any other organelle transport, lysosomes are found in all neuronal domains, such as the soma, dendrites, and axon. How lysosomes are transported in these domains, however, has not been fully understood.

For a long time, the study of axonal transport-associated dynamic process in multifurcated neuron has greatly limited by the technological barrier.[9] Generally, to simplify the axonal transport model, neurons were cultured in a type of microchannel, which was pre-processed into a linear groove with a nanometer width to guide the axon to elongate straight along the groove.[10] Though it is convenient to observe a relatively stable transport along the linear axon, the related conclusion is not enough to be applied to multifurcated complex axons. If this kind of freely orientated multifurcated neuron is cultured on a coverslip pre-treated with cell adhesion molecules, then no space limitation will exist while growth cones move ahead,[11] which provides a naturally morphogenetic neuron model for studying the mechanism of complex axonal transport. Due to the highly complex structure of freely orientated axons with a large number of bends and branches, evaluating the axonal transport principle concerning cargoes passing by the complex axon structure and axon branch point is still challenging.[12,13] Previously, the researcher mainly gathers information via imaging those linear axons and extract data by the means of analyzing fluorescence intensity[14] or kymograph tracking,[15,16]

which is not enough to reveal quantitative motions of axonal transport from the point of anfractuous tracking and instantaneous velocity analysis. Thus, optimized imaging as well as data analysis techniques are still needed to understand axonal transport in freely orientated axons.

In this study, a sparse gene transfection strategy was developed to express and locate fluorescent mCherry in the lysosome of primary neurons. In this way, a single neuron with a mature axon structure can be visualized in the neural network culture derived from the primary neurons. Moreover, the mCherry protein-loaded lysosome can offer a good signal-to-noise ratio for tracking the lysosome-based axonal transport with a single-particle resolution, thus offering a possibility for imaging axonal transport in freely orientated axons. Then, a concise and accurate quantitative algorithm of single-particle velocity, TrackMate, was applied to evaluate the axon transport modes and their reasonable biological interpretations. The combined single-particle tracking and accurate velocity assay revealed a highly heterogeneous and discontinuous transportation process in freely orientated axons. Furthermore, it was also disclosed that multiple physical factors affected the velocity of particle transporting, including the axonal structure and particle size. We believe that combining the advanced single-particle tracking strategy with a flexible and accurate particle velocity analysis will promote a comprehensive understanding of the freely orientated axonal transport mechanism and its biological functions during neuronal development.

2. Material and Methods

2.1. Materials

Laminin, anti-β-tubulin III antibody produced in rabbits were purchased from Sigma-Aldrich (Steinheim, Germany). Lyso-tracker green, tubulin-tracker deep red staining kit for living cells, poly-D-lysine (PDL), penicillin-streptomycin solution (100X) and Hoechst 33342 staining solution were provided from Beyotime (Shanghai, China). Neurobasal medium, sodium pyruvate (100 mM), B-27^{TM}supplement (50X) serum free, L-Glutamine 200 mM (100X) were purchased from Gibco (Thermo Fisher Scientific, Ireland). The goat polyclonal secondary antibody to rabbit IgG-H&L (Alexa Fluor®488) was from Abcam (Cambridge biomedical campus, UK).

2.2. Neuron Culture and transfection

All animal experiments were approved by the Animal Care and Use Committee of the Institutional Animal Committee of Suzhou Institute of Nano-Tech and Nano-Bionics, Chinese Academy of Sciences. Primary neuron culture was performed according to the previous article.[17] Briefly, hippocampal neurons from embryonic day 18 (E18) Balbc rats (Cavens Lab Animal Co., Changzhou, China) were dissected and dissociated by trypsin, the single-cell suspension was plated on 12 mm 0.01% laminine-coated, 0.1% poly-D-lysine precoated coverslips at a density of 2,400 cells/cm^2. The cells were cultured in Neurobasal media including 1% penicillin-streptomycin and 1% L-Glutamine supplemented with 2% B27 and 1% sodium pyruvate. Neuron transfection was operated after 5 days of culture. Each coverslip was renewed with merely Neurobasal media 4 hours in advance, followed by liposome transfection. The amount of vector was applied empirically to allow sparse transfected cells to be visualized.

2.3. Electrophysiology recording

For an electrophysiological experiment, cultured neurons were put in the upright microscope perfusion tank with extracellular bath solution (in mM): 125 NaCl, 2 KCl, 3 $CaCl_2$, 1 $MgCl_2$, 10 HEPES, 30 Glucose, pH=7.3, 300 mOsm. Pipettes had a resistance of 2-7 MΩ when filled with internal solution (in mM): 135 potassium gluconate, 8 NaCl, 10 HEPES, 4 Mg-ATP, 0.4 Na-GTP, 0.6 $MgCl_2$, 0.1 $CaCl_2$, pH=7.25, 295 mOsm. After establishing whole-cell configuration, cell capacitance and access resistance were routinely compensated. All experiments were conducted in a whole-cell patch-clamp configuration. For the recordings of action potentials, a switch to the current clamp was performed. A current was injected to have membrane potentials around -60 mV, then step currents from -40 pA to 50 pA were injected to elicit action potentials by 10 sweeps. Pipettes were prepared by a P-1000 micropipette puller (Sutter Instruments, Hofheim, Germany). Recordings were performed using an EPC10 USB patch-clamp amplifier (HEKA Elektronik, Lambrecht,

Germany), data were digitized at 10 kHz.

2.4. Fluorescent labelling

2.4.1. I mmunofluorescent staining

For immunofluorescent staining, each coverslip with neurons was taken, cleaned with PBS (pH=7.4) 3 times, fixed with 4% paraformaldehyde at room temperature for 10 min, then rinsed with PBS once. The fixed neurons were dipped in 0.1% triton for 10 min, then blocked with 3% serum albumin for 30 min after PBS washing. Removing the blocking solution, samples were covered with the axonal tubulin antibody (1:1000 diluted with PBS) that specifically labels β-tubulin III, standing at 37 for 2 h. Then, the secondary antibody labelled with Alexa Fluor®488 replaced the primary antibody, incubated at 37 for 3 h, followed by 3 times wash, stained with 100 μL Hoechst solution for 5 min. Finally, after washing with PBS, stained neurons were optically imaged under a multichannel microscope (Suzhou NIR-Optics Technology Co., Ltd., China).

2.4.2. Fluorescent labelling of living neurons

Transfected neurons were washed with Neurobasal media three times. Then, live-cell labelling experiments were conducted with microtubule-specific and lysosomal specific fluorescence dye, respectively. The tubulin-tracker dye was diluted with Neurobasal media (1:500) and 200 μL was added to the coverslip. The lyso-tracker dye was diluted with Neurobasal media (1:1000) and added to the coverslip. Neurons were labelled in 37, 5% CO_2 cell incubator for 30 min. After 3 times washed with PBS, 100 μL Hoechst solution was used for nucleus staining. After PBS washing, coverslips were immersed by 1 mL Neurobasal media in the 3 cm diameter dish and observed under an upright microscope. In the experiment, Neurobasal media, PBS, and Hoechst solution were preheated in a water bath at 37 to maintain the normal physiological status of neurons.

2.5. Axonal transport imaging

About two days after transfection, the coverslips were cultured in a Perfusion Chamber RC-26G (Warner Instruments, Hamden, CT) under an upright fluorescence microscope (Suzhou NIR-Optics Technology Co., Ltd., China), the perfusion solution was a neuron culture medium, containing Neurobasal media mixed with 1% penicillin-streptomycin, 1% L-Glutamine, 2% B27 and 1% sodium pyruvate. The microscopic imaging objective is a 60x/1.0 water lens. When operating, first use a low power lens to locate the field of vision, and then a high power lens focuses on the neuronal axon. A 575 nm excitation light from a SpectraX Lumencor solid-state light source (Beaverton, OR, USA) was used to irradiate the sample and the emitted light through a filter into the QImaging Retiga R3 camera (Burnaby, BC Canada). Fluorescent images were acquired in TIFF format by the Ocular 2.0 software that matched the camera and recorded at the video mode with an exposure time of 500 ms. The recording duration depended on the time of availing axonal transport observation.

2.6. Imaging analysis

2.6.1. Axon width measurement

The axon width was measured by Fiji (open source https://fiji.sc/) and Origin software (Origin Lab Corporation, Northampton, Ma, USA). Firstly, the ordinal operation ImageJ-Analytic-Set Scale was used to adjust the scale bar, and then ImageJ-Analyze-Plot Profile click could extract the fluorescence intensity value (gray value) of neuronal axons. These data were stored in a text file and then imported into the Origin to draw a line chart. Ordinal click Analysis-Fitting-Nonlinear Curve Fit-Open Dialog-Gauss was used to perform the Gaussian fitting. Finally, the fitted curve was selected, followed by orderly clicking Analysis-Mathematics-Integrate-Open Dialog, checked "connect endpoint as a baseline", and then the "dx" in the Results Log window was the width of axons in the raw image.

2.6.2. Instantaneous velocity measurement

The instantaneous velocity was analyzed by Fiji (ImageJ) and Origin software. First, ordinal click ImageJ-Process-Subtract Background could decrease the background noise of original images and highlight the fluorescence signal. Then, click ImageJ-Analysis-Set Scale to set the scale bar. After that, the program files of KymographClear Plugin and TrackMate Plugin downloaded from ImageJ's official website should be directly imported into the plugins folder within ImageJ software, and ImageJ was restarted for subsequent operation.

Importing the refined image, pulling down the right arrow "More Tools" menu, selecting KymographClear 2.0.0, and sequentially operating Make a segmented line Tool [F3] to manually select the region of interest (ROI) area, SplineTool [F4] to smooth freehand lines, Kymograph generation Tool [F5] to record the kymograph of specific axons. After randomly circling a piece of the background area, the background value was obtained by the Background Tool shortcut key [F6], which was automatically stored in the Kymograph folder to calibrate the fluorescent signal. In turn opening KymographDirect 2.1 software, importing Color Coded Directions named picture in Kymograph folder, clicking Tools-Parameters, inputting and affirming Time Per Frame (ms) and Pixel Size (μm), then adjusting Intensity threshold to ensure that moving particle tracks were tagged, finally, right-clicking upper-right Particle velocities-Times graph to save as a text file.[18] Later data processing was done in Origin software.

Another analysis method also started at importing the refined image. Firstly, selecting Plugins-Tracking-TrackMate to enter the calibration parameter setting window, input the value of Pixel Width (μm) and Time Interval (s). Then, the default settings were applied, such as LoG Detector, HyperStack Displayer and Simple LAP Tracker, and the parameters were adjusted empirically to properly select the target particles. Finally, clicking Analysis in the Display options window, the exported features of all Tracks were saved as a text file. Data analysis and visualization were done in Origin software. The detailed operation could refer to the relevant reference.[19]

2.7. Statistical analysis

This study used Origin2018 (Origin Lab Corporation, Northampton, Ma, USA) for data processing and analysis. Parameter values were expressed as mean ± standard deviation (?x +- S). ANOVA was used for one-way data analysis. $^{***}P < 0.01$ was considered as a statistically significant difference.

3. Results and discussion

3.1. Neuron growth and transfection

To obtain neurons with mature axon and dendritic structure, primary hippocampal neurons were isolated and cultured for 5 days (Figure S1). Immunofluorescence assay revealed that the neurons were all Tuj1-positive and possessed a mature axon of approximate 0.74 μm width (Figure S1A). After that, the Tuj1-positive neurons were transfected to express mCherry proteins by a plasmid encoding CMV promoter-driven mCherry gene (Figure 1A). A continuous fluorescence imaging of a single neuron found that mCherry protein could be detected and evenly distributed in the cell soma and axon of neurons at 48 h after transfection (Figure 1B and Figure S1B). And then the clear granular fluorescence signal was visible between 60 h and 72 h, suggesting the formation of mCherry aggregations during this period. Finally, the fluorescence signal of the whole neuronal axon became discrete at 78 h. These results suggested an optimal axonal transport observing window between 60 h and 72 h after transfection, considering that the over-expression of mCherry protein for more than 72 h would affect the physiological state of neurons. It also demonstrated that the sparse transfection strategy can serve as a facile strategy to produce and image fluorescent protein aggregates in a single living neuron.

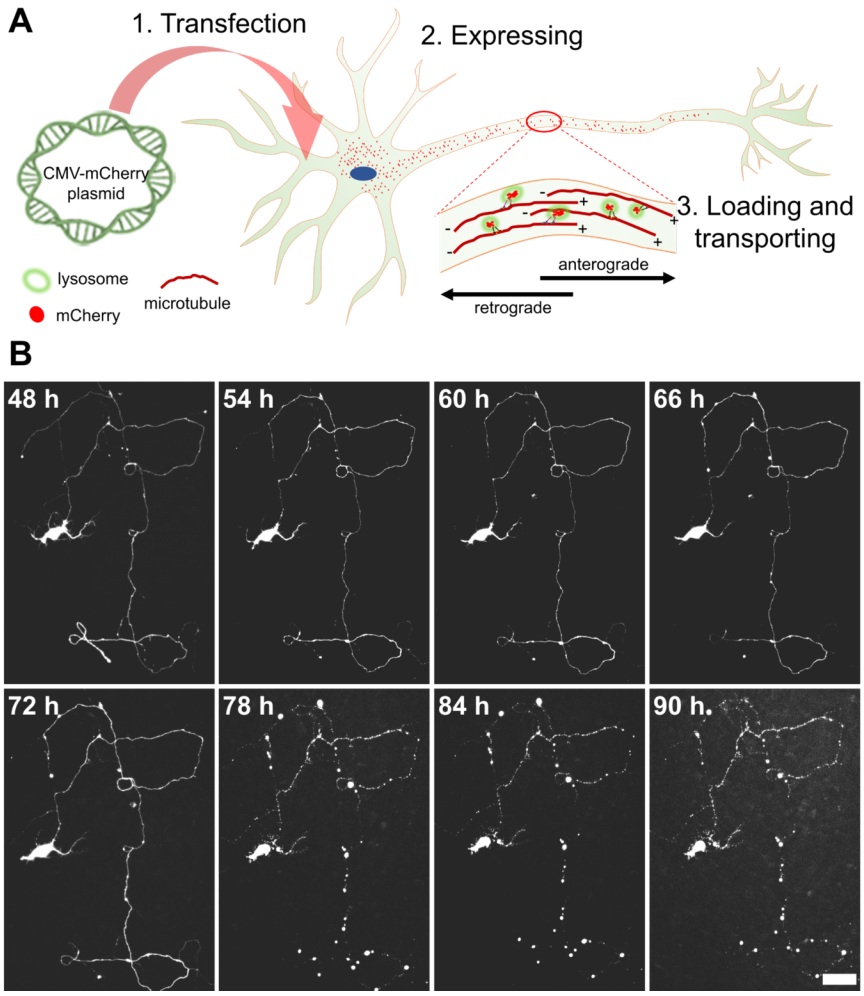

Figure 1. Transfection of primary hippocampal neurons. (A) Scheme of transfection, expression and transporting of mCherry in neurons. (B) Fluorescence images of transfected primary hippocampal neurons. Scale bar: 10 μm.

3.2. Colocalization of mCherry proteins, axonal lysosomes and tubulin

To figure out how mCherry protein granules formed and moved, we first analyzed the colocalization between the mCherry signal and lysosome signal in the axon. Notably, the fluorescence of mCherry highly merged with the lysosomal signal (Figure 2), indicating the mCherry protein granules were formed by wrapping the mCherry in the lysosome. This result agrees with previous founding that the over-expressed GFP-like proteins were accumulated in the lysosome of cells.[20] It is known that lysosomes are responsible for endocytic and autophagic components degradation and transportation, thus maintaining cellular homeostasis in neurons.[21] Thereby, the formation of lysosomes with fluorescent mCherry may attribute to the strategy of removing extra proteins via axonal transport to maintain the homeostasis of substances in axons.[22] In axons, the microtubule serves as a basic cytoskeleton for neuronal polarity, axon growth, branching and axonal transport.[23] To further confirm whether mCherry protein granules can be loaded on microtubules, we analyzed the colocalization between the mCherry and microtubule. It was found that the mCherry protein granules were intermittently distributed on the microtubule skeleton of the axon (Figure 2C). These results suggested the over-expressed mCherry were able to be gradually wrapped in the lysosome and loaded

on microtubules for axonal transport imaging. And the sparse labelling strategy can be used as a convenient model for the study of lysosomal transport in axons of freely orientated neurons.

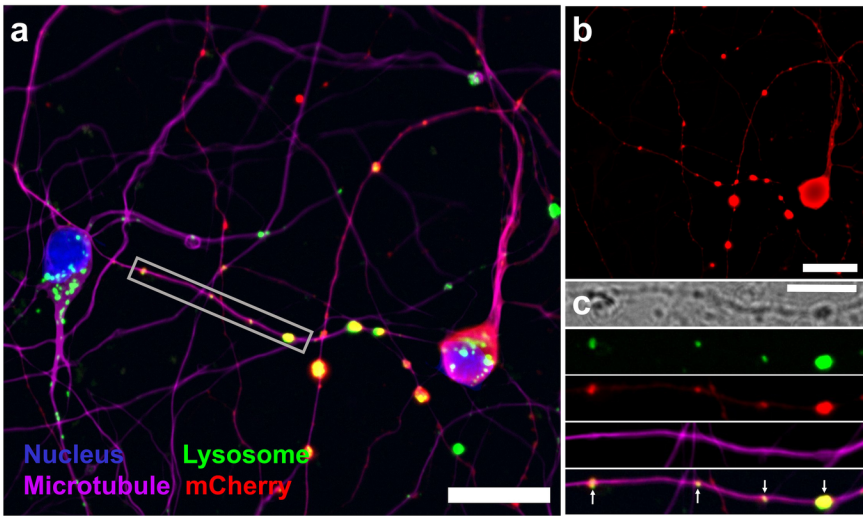

Figure 2. Fluorescence imaging of mCherry, lysosome and tubulin of transfected neurons. (A) A representative result of neurons labeled by Hoechest (blue, nucleus), lyso-tracker dye (green, lysosome), tubulin-tracker dye (pink, microtubule) and mCherry (red). Scale bar: 20 μm. (B) The distribution of mCherry proteins in picture A. Scale bar: 20 μm. (C) Magnified image of ROI indicated in picture A. Scale bar: 10 μm.

3.3. Electrophysiological activity analysis

The electrical activity of neurons is an extensive integration of neuronal ion channel function. These ion channel proteins are transported by axons to specific locations to establish neuronal polarity and influence synaptic plasticity.[24]Hence, electrophysiological activity is regarded as a key indicator to inspect whether the neuron is physiological disordered or diseased.[25,26] To explore the effect of gene transfection on the physiological activity of neurons, the electrophysiology assays of non-transfected (Figure 3A) and transfected (Figures 3B and 3D) primary cultured neurons were conducted. Membrane potential was maintained at -60 mV with a current clamp model via adjusting injection current properly range from -10 pA to -15 pA. The stimulus program was run successively from -20 pA to 70 pA by 10 pA steps (Figure 3C). We found that the induced action potential of primary cultured hippocampal neurons took place when the injection current was 30 pA. With the injected current going up, the frequency of evoked action potentials increases (Figure 3E). In the transfected neurons, a similar electrophysiological result was observed (Figure 3F), indicating that the expression of mCherry protein did not affect the physiological state of neurons after transfection. Moreover, the electrophysiological results in combination with the results of the entire axon structure (Figure 1) and microtubule skeleton architecture (Figure 2B), as well as unaffected Tuj-1 expression (Figure S1) after transfection suggested the transfection strategy has a minimal side effect on the physiological state of neurons during the imaging period.

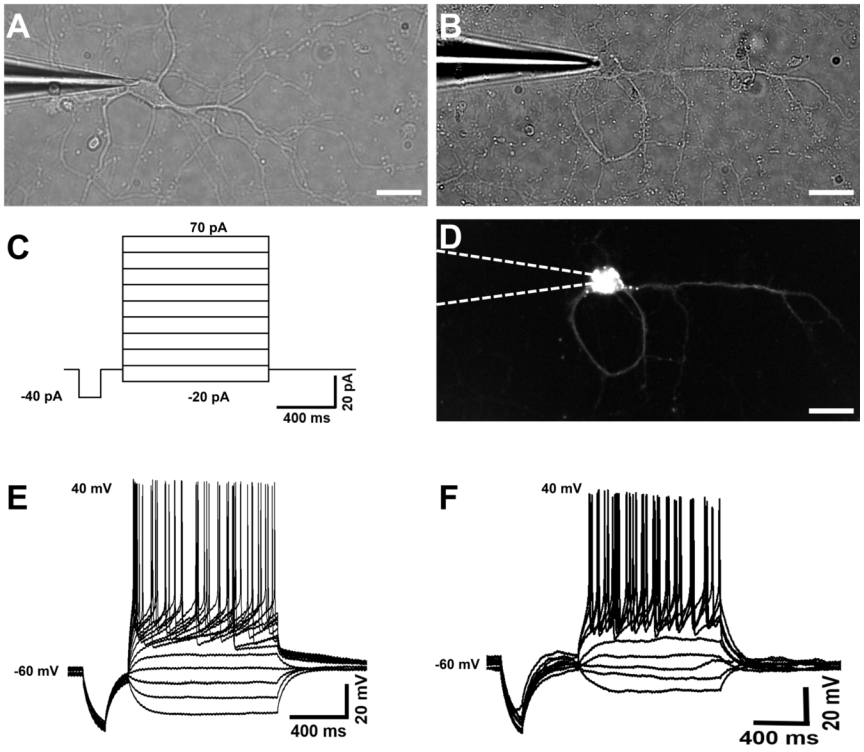

Figure 3. The electrophysiological properties of primary neurons transfected or untransfected with plasmids. (A) Untransfected neuron and (B) transfected neuron under the whole-cell patch-clamp recording. (C) A current injection procedure. (D) Fluorescence imaging of transfected neurons. Dotted lines indicate the position of the micropipette. (E) The evoked action potentials correspond to untransfected neurons (A). (F) The evoked action potentials correspond to transfected neurons (B). Scale bar: 20 μm.

3.4. Axonal transport imaging in freely orientated axons

In addition to the above work for fluorescence imaging, we further undertook axonal transport imaging in freely orientated axons. Unlike the microchannel-culturing method,[10,27] coverslip-culturing method provided a freely orientated growth pattern for natural morphogenesis owing to no space limitation in the culture environment, thus obtaining multifurcated axons with mCherry located at lysosomes. Hence, four axonal transport models were observed. The first one is the forward or backward transport model (Figure 4A and Video S1) in a ring-like axon, most of the particles moved forward while others moved backwards. One classic interpretation comes from the tug-of-war model[28] that mainly contained two kinds of motor proteins, dyneins and kinesins, which determine the direction by integrating the force from a mole ratio between these two proteins, retrograde or anterograde.[29] The second model is the stop-and-go model in which particles previously moved then suddenly came to rest together at a certain moment (Video S2). In Figure 4B, particles were moving before 215 s, and keeping still for the rest of the time. On the one hand, we attributed this static state to the discontinuity of ATP supply because axonal transport is dependent on the supply of ATP to drive the motor proteins.[30] On the other hand, axonal transport-related regulatory proteins in axons may also contribute to stop or start the transport of particles in the axons.[31]

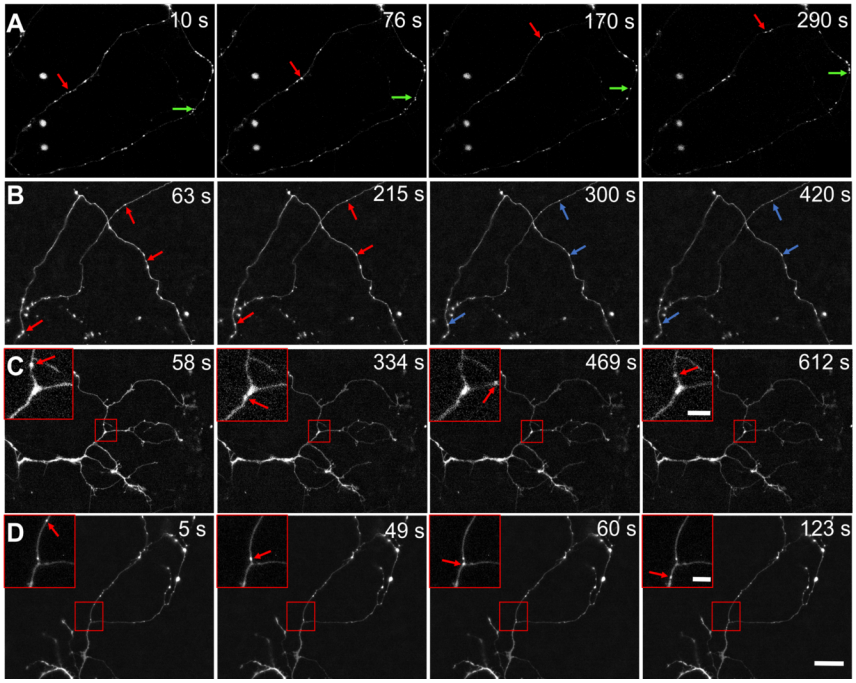

Figure 4. Various transporting behaviors among freely orientated axons. (A) Forward or backward transport model. Red arrow: forward moving, green arrow: backward moving. (B) Stop-and-go model. Red arrow: moving particle, blue arrow: static particle. (C) Repeated back-and-forth transport model. Red arrow: moving particle. (D) Cross-branch transport model. Red arrow: moving particle. Outer scale bar: 20 μm. Inner scale bar: 5 μm.

Another two models are related to axon branches, one is repeated back-and-forth transport model (Figure 4C and Video S3), a particle moved back-and-forth across the axon branching point several times, and the other one is the one-way cross-branch transport model (Figure 4D and Video S4), a particle came across the axon branching point without direction change. Unlike linear-orientated axons, collateral branching derives from a reorganization of microtubule arrays[32] thereupon making multifurcated axons more intractable to understand in axonal transport. We suggested that the original reorganized microtubules at the branch point were not as orderly as that in the linear axons,[23,33] and the proteins that are responsible for shunt migration interfered with each other, which may affect the direction or velocity of moving particles. These results suggested the axonal transport route in freely orientated axons is more complicated than that in the linear-orientated axons, since there are a lot of bends and branch transportation routes in freely orientated axons.

3.5. Single-particle tracking and velocity analysis

To achieve an accurate particle velocity analysis of lysosomal transport, we selected a recently published algorithm TrackMate[19] for single-particle tracking and compared it with the mainstream algorithm KymographClear[18] for the same goal. It is previously reported that the velocity analysis by KymographClear is not continuous because the software exclusively identifies moving particles and does not record the static velocity at the same time,[34] and the static velocity in the whole period needs to be uniformly set to zero to draw in a diagram. In contrast, the velocity analysis energized by the TrackMate algorithm can recognize the target particle and record its velocity in the whole period no matter which state of motion it is, moving or stationary. Unless the moving particle is exactly stationary, the recorded speed should always be greater than zero. In other words, KymographClear only obtains the velocity of moving particles (the static velocity is not recorded) while TrackMate can extract the velocity in a whole period (both moving

and static velocities are recorded).

As shown in Figure 5A, the location of particle a was recorded at time t_1, t_2,..., $t_7$respectively, and the location-time diagram was drawn in the red coordinate axis. By exerting the KymographClear algorithm, all the positions of particle a were marked at time t instantaneously, then its track would be depicted in Figure 5C. The kymograph record starting from the upper left corner is particle a's track, another two lines represent the other two particles that can't be excluded but analyzed at the same time. Then, we further obtained the velocity-time diagram drawn in Figure 5D (marked in red) after setting the speed of the unrecognized motion to zero. Figure 5B shows the initial analysis result of particle a with the TrackMate algorithm. The green line referred to the track of particle a, and the tracking length was measured as 25.67 μm. The purple mark meant several other moving particles were identified at the same time. Eventually, the velocity-time diagram of particle a was shown in Figure 5D (marked in green) in a whole period without data interrupt. We then compared the subtle difference of velocity data extracted by these two algorithms. One point to state is that the average velocity of particle a calculated by these two algorithms is similar, approximately 0.103 μm/s (KymographClear algorithm) and 0.094 μm/s (TrackMate algorithm) (Figure 5D), suggesting that these two algorithms work well for average velocity analysis. However, these two algorithms are significantly different in the analysis of instantaneous velocity. As revealed by the velocity-time diagram (Figure 5D), the lysosomal transport in the axon is a highly heterogeneous and discontinuous transportation process with numerous velocity fluctuations. TrackMate algorithm shows more concise and accurate than the KymographClear algorithm for single-particle velocity assay. For example, three velocity fluctuations around 50 s were recorded by TrackMate (green line), while only one velocity change was recorded by KymographClear (red line). Moreover, after 100 s, the red line tended to flatten out, while the green line still showed several significant changes (three spikes) with a significant unsmooth curve. It is suggested that there is a brief unbalance between motor proteins that respond to the dynamic concentration changes of kinesins and dyneins, or the frequency of spikes represent other axonal transport features. These phenomena can just be visualized by the TrackMate algorithm. Undoubtedly, we obtained the same results by analyzing the motion of particle b (Figure S2). It proves that, on the premise of ensuring the consistent average velocity of particles, the TrackMate algorithm can better retain the velocity fluctuations and provide better fidelity than the KymographClear algorithm in restoring the motion details.

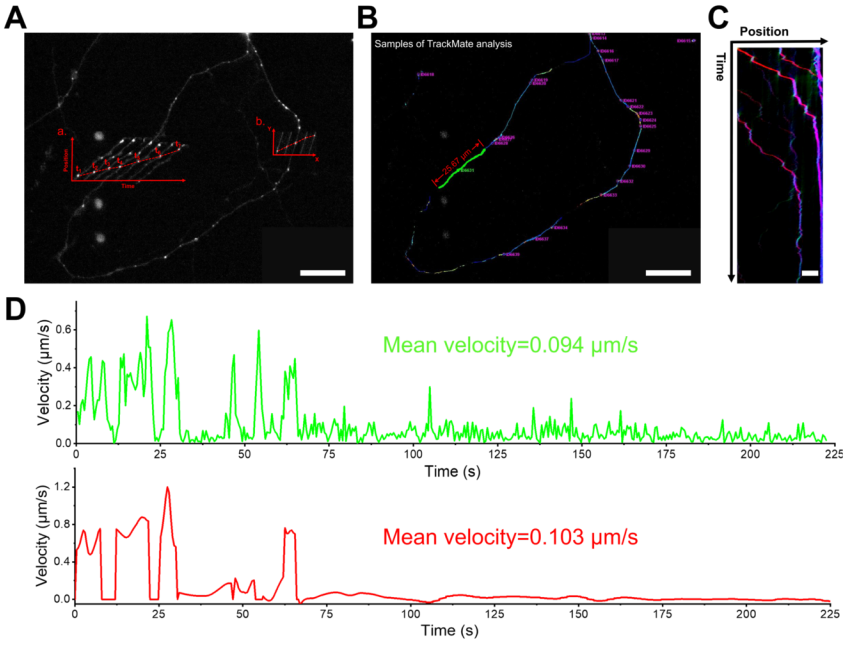

Figure 5. Lysosomal transport velocity analysis by comparing TrackMate and KymographClear algorithm. (A) A diagram of the motion of particles a and b. Scale bar: 20 μm. (B) A typical screenshot of the TrackMate algorithm during analyzing the velocity of axonal transport. The green line represents the trajectory of target particle a. Scale bar: 20 μm. (C) The result of the KymographClear algorithm about particle a. Red color notes forward-moving while green color notes backward moving, and blue color notes static. Scale bar: 5 μm. (D) The velocity-time diagram based on TrackMate and KymographClear algorithms, respectively.

In addition, in terms of the complexity of application operation, the KymographClear algorithm can only extract the motion velocity of one target particle at a time, while the TrackMate algorithm can analyze the motion condition of multiple target particles at the same time, which makes the operation more convenient and efficient. To sum up, compared with the KymographClear algorithm, the merits of the TrackMate algorithm can promote more concise and accurate analyses of lysosomal transport and a better understanding of the axonal transport mechanisms.

3.6. Factors involved in the velocity of axonal transport in freely orientated axons

After confirming that the TrackMate algorithm can be used as a concise and efficient tool for axonal transport analysis, we applied it to single-particle velocity analysis nearby axon branch point and multiple particle velocity analysis for axonal transport interpretation. Judging from the four stages in which moving particles passing by axonal branch (Figure 6A), the first stage is in slow motion (˜0.106 μm/s), the velocity of the second stage is accelerated (˜0.217 μm/s) and it seems to suddenly slow down while encountering with another particle. The velocity of the third stage is the slowest (0.024 μm/s) when it reaches the branching point. After passing by the axonal branch, the fourth stage velocity remains ˜0.067 μm/s (Figure 6B). All these velocities illustrate that transportation of cytoplasmic protein mCherry wrapped in the lysosome belongs to a slow transport.[35] Then, we made a statistical analysis of the particle velocity before and after the branching point (Figure S3A), and it is obvious that the particle velocity before the branching point is higher than that after the branching point. The different microtubule arrangements nearby the branching point may bring about a different integrated force exerted on lysosomes during transportation.[23] These results suggested the velocity of axonal transport is partly dependent on the structure of axons. To further explore whether the size of particles affects the axonal transport velocity, we analyzed the velocity of 17 target particles in Figure 6C (Table S1) and confirmed the negative correlation between particle sizes and velocities, when the particle size ranged from 0.644 μm to 0.721 μm, the velocity could decrease from 0.439 μm/s to 0.067 μm/s (Figure 6D).

Moreover, at the molecular level, we provide a possible reason why larger particles move slower and most of the movement is in the same direction. First, the lysosomal transport homeostasis is generally maintained by a mole ratio of dynein to kinesin motors in the tug-of-war model.[7,29] Without considering the fusion between lysosomes, once particles get bigger, more sparse ligand proteins anchor in the lysosome membrane, and fewer chance particles have to be recognized by dynein/kinesin motors. Hence, the mole ratio of dynein to kinesin motors becomes unbalanced, and the bidirectional lysosomal transport tends to be unidirectional. It is also possible that lysosomes are in the one-way transport stage due to their developmental state.[15,36,37] Second, we simplify the tug-of-war model to one-way transportation for a concise explanation of moving velocities.[29] We have inferred those particles will have fewer chances to be recognized by kinesin motors if they get bigger, therefore the force from kinesin motor decreases. On the other hand, the increased load caused by larger particles further hinders the motion of kinesin protein, which makes the movement speed slower than smaller particles.

But this movement correlation doesn't exist once we expanded the applicability to axons of different neurons, we found the velocity and diameter of particles in new statistics were irregular (Figure S3B, Video S1-S5, and Table S2). Maybe in different cells, the subtle microenvironment of axonal transport, such as microtubule density and arrangement,[23] motor protein quantity, regulatory protein concentration etc., makes a uniform and reasonable judgement intractable.[38]

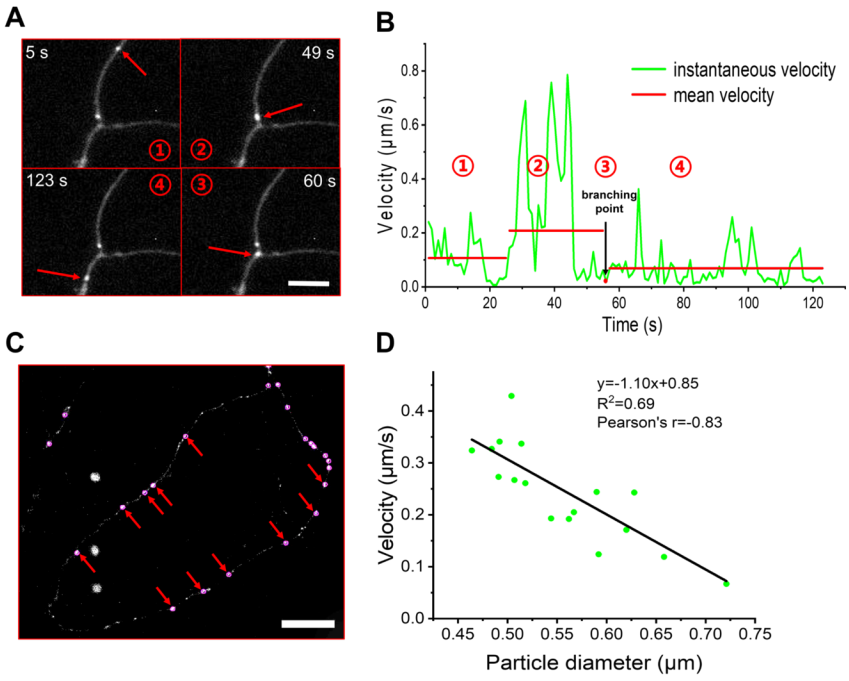

Figure 6. Axonal transport analysis with TrackMate algorithm. (A) Single-particle velocity analysis during four phases in cross-branch transport. Scale bar: 5 μm. (B) The velocity-time diagram about the particle showed in (A). (C) Target particles selected from ring-like axonal transport. Scale bar: 20 μm. (D) The correlation analysis between velocity and diameter of particles marked in (C).

4. Conclusions

We successfully combine sparse neuron labelling, single-particle fluorescence imaging with a concise and accurate quantitative algorithm of single-particle velocity (TrackMate) for precisely tracking and quantifying various lysosomal transport in freely orientated axons. Thus, several axonal transport models were found, including forward or backward transport model, stop-and-go model, repeated back-and-forth transport model, and cross-branch transport model. Furtherly, this study also revealed the velocity of single-particle transporting in freely orientated axons was a highly heterogeneous and discontinuous transportation process. Moreover, the axonal structure and particle size were all found to affect the velocity of particle transporting in freely orientated axons. We believe that the facile axonal transport assay may be furtherly served as a kind of physiological steady-state parameter assay to investigate neuronal development and axonal transport-related diseases.

Though we have introduced TrackMate to accurately analyze single or multiple particle velocity at the same time, we can't get a better understanding of the phenomenon that the velocity change during or after the particle passing by the axon branching point due to the insufficient temporal-spatial resolution to identify a single molecule in the axon. Thus, the TrackMate together with an advanced single-molecule imaging microscope may offer a more accurate velocity analysis to disclose the molecular mechanisms involved in axonal transport during neuronal development or diseases. On the other hand, this study only studied the freely orientated neurons cultured on a coverslip due to the limited tissue penetration depth of mCherry-based fluorescence imaging. We believe that TrackMate in combination with a near-infrared fluorescence imaging-based axonal transport tracking technique[39,40] may offer a possibility for exploring axonal transport in tissues or living animals.

Acknowledgements

This work was supported by the National Key Research and Development Program (2017YFA0205503), the National Natural Science Foundation of China (Grant No. 21778070, 22177128, 21934007), Chinese Academy of Sciences (Grant No. XDB32030200, 121E32KYSB20180021, ZDBS-LY-SLH021), the Youth Innovation Promotion Association of Chinese Academy of Sciences, the Science and Technology Project of Suzhou (Grant No. SZS201904). The authors thank Suzhou NIR-Optics Technology Co., Ltd. for its instrumental and technique support on the fluorescence imaging.

Conflict of interest

The authors declare that they have no known competing financial interests or personal relationships that could have appeared to influence the work reported in this paper.

Author Contributions

Y.L., Y.L.: Conceptualization, investigation, methodology, validation, visualization, software, writing the original draft and editing. Z.T., Y.C., D.H., W.F.: Formal analysis, investigation and editing. Y.Z. C.L.: Funding acquisition and draft editing. G.C.: Conceptualization, formal analysis, funding acquisition, supervision, writing the original draft and editing; Q.W.: Conceptualization, project administration, supervision, funding acquisition.

Data availability statement

All data that support the findings of this study are included within the article (and any supplementary files).

References

[1] L. Guillaud, S. E. El-Agamy, M. Otsuki, M. Terenzio,*Front. Molec. Neurosci.* **2020** , *13* , 17.

[2] M. P. Sheetz, *Cell Struct. Funct* . **1996** ,*21* , 369.

[3] Y. Yonekawa, A. Harada, Y. Okada, T. Funakoshi, Y. Kanai, Y. Takei, S. Terada, T. Noda, N. Hirokawa, *J. Cell Biol.***1998** , *141* , 431.

[4] L. Wang, A. Brown, *Mol. Biol. Cell* **2001** ,*12* , 3257.

[5] V. K. Lund, M. D. Lycas, A. Schack, R. C. Andersen, U. Gether, O. Kjaerulff, *Cell Rep.* **2021** , *35* , 25.

[6] C. Rosa-Ferreira, S. Munro, *Dev. Cell* **2011** ,*21* , 1171.

[7] J. Pu, C. Schindler, R. Jia, M. Jarnik, P. Backlund, Juan,*Dev. Cell* **2015** , *33* , 176.

[8] G. G. Farias, C. M. Guardia, R. De Pace, D. J. Britt, J. S. Bonifacino, *Proc. Natl. Acad. Sci. U. S. A.* **2017** ,*114* , E2955.

[9] J. N. Sleigh, A. Vagnoni, A. E. Twelvetrees, G. Schiavo,*F1000Research* **2017** , *6* , 200.

[10] A. M. Taylor, S. Menon, S. L. Gupton, *Lab Chip***2015** , *15* , 2781.

[11] W. S. Chen, C. Y. Yueh, Y. A. Huang, E. Hwang, *Neurosci. Res.* **2011** , *70* , 118.

[12] S. Maday, E. L. F. Holzbaur, *Dev. Cell* **2014** ,*30* , 71.

[13] G. Plucinska, D. Paquet, A. Hruscha, L. Godinho, C. Haass, B. Schmid, T. Misgeld, *J. Neurosci.* **2012** , *32* , 16203.

[14] P. Guedes-Dias, J. J. Nirschl, N. Abreu, M. K. Tokito, C. Janke, M. M. Magiera, E. L. F. Holzbaur, *Curr. Biol.***2019** , *29* , 268.

[15] S. Maday, K. E. Wallace, E. L. F. Holzbaur, *J. Cell Biol.* **2012** , *196* , 407.

[16] X. Ye, T. Feng, P. Tammineni, Q. Chang, Y. Y. Jeong, D. J. Margolis, H. Cai, A. Kusnecov, Q. Cai, *J. Neurosci.***2017** , *37* , 2639.

[17] M. Zeng, Y. Shang, Y. Araki, T. Guo, R. L. Huganir, M. Zhang,*Cell* **2016** , *166* , 1163.

[18] P. Mangeol, B. Prevo, E. J. G. Peterman, *Mol. Biol. Cell***2016** , *27* , 1948.

[19] J. Y. Tinevez, N. Perry, J. Schindelin, G. M. Hoopes, G. D. Reynolds, E. Laplantine, S. Y. Bednarek, S. L. Shorte, K. W. Eliceiri,*Methods* **2017** , *115* , 80.

[20] H. Katayama, A. Yamamoto, N. Mizushima, T. Yoshimori, A. Miyawaki, *Cell Struct. Funct* . **2008** , *33* , 12.

[21] R. A. Nixon, D. S. Yang, J. H. Lee, *Autophagy***2008** , *4* , 590.

[22] F. B. Tamar, J. C. Roney, C. Xiu-Tang, L. Sunan, S. R. Cuddy, S. Zu-Hang, *Autophagy* **2020** , *16* , 167.

[23] T. J. Lee, J. W. Lee, E. M. Haynes, K. W. Eliceiri, M. C. Halloran, *Front. Cell. Neurosci.* **2017** , *11* , 14.

[24] H. C. Lai, L. Y. Jan, *Nat. Rev. Neurosci.* **2006** ,*7* , 548.

[25] L. K. Liem, J. M. Simard, Y. M. Song, K. Tewari,*Neurosurgery* **1995** , *36* , 382.

[26] B. Buisson, M. Gopalakrishnan, S. P. Arneric, J. P. Sullivan, D. Bertrand, *J. Neurosci.* **1996** , *16* , 7880.

[27] K. Zhang, R. F. Ben Kenan, Y. Osakada, W. Xu, R. S. Sinit, L. Chen, X. Zhao, J. Y. Chen, B. Cui, C. Wu, *J. Neurosci.***2013** , *33* , 7451.

[28] P. Guedes-Dias, E. L. F. Holzbaur, *Science***2019** , *366* , 199.

[29] A. G. Hendricks, E. Perlson, J. L. Ross, H. W. Schroeder, M. Tokito, E. L. F. Holzbaur, *Curr. Biol.* **2010** , *20* , 697.

[30] S. Maday, A. E. Twelvetrees, A. J. Moughamian, E. L. F. Holzbaur, *Neuron* **2014** , *84* , 292.

[31] R. H. Lee, C. S. Mitchell, *J. Theor. Biol.***2015** , *370* , 39.

[32] A. Ketschek, S. Jones, M. Spillane, F. Korobova, T. Svitkina, G. Gallo, *Dev. Neurobiol.* **2015** , *75* , 1441.

[33] C. C. Winkle, K. L. Taylor, E. W. Dent, G. Gallo, K. F. Greif, S. L. Gupton, *Dev. Neurobiol.* **2016** , *76* , 1293.

[34] J. D. Fenn, C. M. Johnson, J. Peng, P. Jung, A. Brown,*Cytoskeleton* **2018** , *75* , 22.

[35] S. Roy, *Neuroscientist* **2014** , *20* , 71.

[36] T. Nakata, N. Hirokawa, *J. Cell Biol.* **1995** ,*131* , 1039.

[37] K. Ibata, M. Yuzaki,*Neurosci. Res* . **2021** ,*167* , 38.

[38] S. Roy, *Curr. Opin. Neurobiol* . **2020** , *63* , 87.

[39] G. Chen, Y. Cao, Y. Tang, X. Yang, Y. Liu, D. Huang, Y. Zhang, C. Li, Q. Wang, *Adv. Sci* . **2020** , *7* , 27.

[40] C. Li, G. Chen, Y. Zhang, F. Wu, Q. Wang, *J. Am. Chem. Soc* . **2020** , *142* , 14789.